Available online at www.sciencedirect.com
ScienceDirect
Journal of Solid State Chemistry 180 (2007) 3111–3120
JOURNAL OF SOLID STATE CHEMISTRY
www.elsevier.com/locate/jssc

Synthesis and characterization of four new metal 5-phosphonoisophthalates discovered by high-throughput experimentation

Sebastian Bauer, Norbert Stock*

Institute of Inorganic Chemistry, Christian-Albrechts-University, Otto-Hahn-Platz 6/7, D 24098 Kiel, Germany

Received 29 June 2007; received in revised form 8 August 2007; accepted 31 August 2007
Available online 8 September 2007

Abstract

A new ligand, 5-diethylphosphonoisophthalic acid ($(HOOC)_2C_6H_3$-$PO_3(C_2H_5)_2$, H_2Et_2L), for the hydrothermal synthesis of inorganic–organic hybrid compounds was prepared and characterized by NMR-spectroscopy. Its in situ hydrolysis leads to the corresponding 5-phosphonoisophthalic acid ($(HOOC)_2C_6H_3$-PO_3H_2, H_4L). Applying high-throughput methods, different di- and trivalent metal salts for the synthesis of crystalline metal phosphonates based on H_2Et_2L have been screened. From the resulting discovery library, single-crystals of four new compounds, $[Sm_2(H_2O)_4(H(OOC)_2C_6H_3$-$PO_3)_2]\cdot 2H_2O$ (**1**), $[Cu_3(H_2O)(H(OOC)_2C_6H_3$-$PO_3)_2]\cdot 2H_2O$ (**2**), $Ca_2(H_2O)[H(OOC)_2C_6H_3$-$PO_3H]_2$ (**3**), and $Ba_2(H_2O)_3(OOC)_2C_6H_3$-$PO_3$ (**4**), have been isolated. The single-crystal structure determination of the title compounds shows H_4L to be a versatile ligand, exhibiting different types of coordination modes between the functional groups and the metal ions. A comparison of the structural features of the title compounds shows a varying degree of M–O–M connectivities. Thus, isolated metal–oxygen clusters (compounds **1** and **2**), infinite M–O–M chains (compound **3**), and infinite M–O–M layers (compound **4**) are observed. The title compounds **1**, **2**, and **3** were further characterized by IR-spectroscopy, TG-, EDX-, and elemental chemical analysis.

Keywords: Metal phosphonates; High-throughput methods; Combinatorial chemistry; Phosphonocarboxylic acid; Inorganic–organic hybrid compounds; Crystal structure

1. Introduction

Inorganic–organic hybrid materials have raised a lot of interest not only in academia but also in industry. This is due to their fascinating structural chemistry and their potential application i.e. in the fields of gas separation and storage, as well as catalysis, or sensors [1–4]. The chemistry of metal carboxylates is well developed due the existence of secondary building units which can be connected by organic linkers to form metal-organic frameworks (MOFs). This extremely successful strategy is often referred to as "reticular synthesis" [5] or "scale chemistry" [6]. In this aspect, the use of 1,3,5-benzenetricarboxylic acid (BTC, $C_3H_3(COOH)_3$) has been very successful, leading for example to fascinating materials such as HKUST-1 ($Cu_3(C_6H_3(COO)_3)_2(H_2O)_3$) [7] or MIL-100 ($Cr_3F(H_2O)_3O[C_6H_3(COO)_3]_2\cdot nH_2O$ ($n\sim 28$) [8]. However, in metal phosphonate chemistry, there seem to be left many unknown factors for controlling the crystal structure one being the high coordination flexibility of the phosphonate group. Nevertheless, metal phosphonates are promising candidates for the synthesis of inorganic–organic hybrid open-framework materials [4]. We are interested in the systematic investigation of polyphosphonic and phosphonocarboxylic acids as starting compounds for the synthesis of new metal phosphonates [9–12]. The goal is to establish structural and synthetic trends in these systems for a better understanding of metal phosphonate chemistry. Thus, we have established high-throughput (HT) methods in our group, which allow the systematic and rapid investigation of reactions under solvothermal conditions. [12–15]

*Corresponding author. Fax: +49 431 880 1775.
E-mail address: stock@ac.uni-kiel.de (N. Stock).

0022-4596/$ - see front matter © 2007 Elsevier Inc. All rights reserved.
doi:10.1016/j.jssc.2007.08.026

Recently, we started an investigation of the successive exchange of the carboxylic acid groups by phosphonic acid groups in BTC in order to study the effect on the resulting structures. Herein, we report on the synthesis of the new ligand, 5-diethylphosphonoisophthalic acid ($(HOOC)_2C_6H_3$-$PO_3(C_2H_5)_2$, H_2Et_2L). The in situ hydrolysis leads to the formation of the corresponding 5-phosphonoisophthalic acid ($(HOOC)_2C_6H_3$-PO_3H_2, H_4L) which reacts with the metal ions Sm^{3+}, Cu^{2+}, Ca^{2+}, and Ba^{2+} to form four new metal phosphonates.

2. Experimental section

$BaCl_2 \cdot 2H_2O$ (Merck, >99%), $CuCl_2 \cdot 2H_2O$ (Merck, 99%), $Co(OAc)_2 \cdot 4H_2O$ (Aldrich, >98%), $CaCl_2 \cdot 2H_2O$ (Merck, >99%), $AlCl_3 \cdot 6H_2O$ (Fluka, >99%), $SmCl_3 \cdot 6H_2O$ (Strem Chemicals, 99.9%), NaOH (Merck, ⩾99%), $KMnO_4$ (Grüssing, 99%), Na_2CO_3 (Fluka, ⩾99%), and 1-bromo-3,5-dimethylbenzene (Alrich, 97%) have been used without further purification.

2.1. Synthesis of $(HOOC)_2C_6H_3$-$PO_3(C_2H_5)_2$ (H_2Et_2L)

5-Diethylphosphonoisophthalic acid ($(HOOC)_2C_6H_3$-$PO_3(C_2H_5)_2$, H_2Et_2L), was synthesized in two steps (Fig. 1). 1-Diethylphosphono-3,5-dimethylbenzene (**II**) was prepared based on a procedure described in the literature [16]. To a suspension of 2.50 g (13.5 mmol) 1-bromo-3,5-dimethylbenzene (**I**) and 0.576 g (0.264 mmol) anhydrous $NiBr_2$, 2.92 g (17.5 mmol) $P(OEt)_3$ were carefully added dropwise within 30 min under nitrogen atmosphere at 160 °C. The formed Et-Br was removed from the reaction vessel by applying a nitrogen flow. The resulting reaction product was dissolved in 200 ml ethylacetate, and washed with water three times. The organic phase was dried over anhydrous $MgSO_4$. Ethylacetate and $P(OEt)_3$ were removed in vacuo (10 mbar, 65 °C). The resulting crude product was purified by column chromatography (silica, ethylacetate:MeOH = 10:1). After removing the solvent, 2.13 g (8.78 mmol, 65% yield) of a yellowish

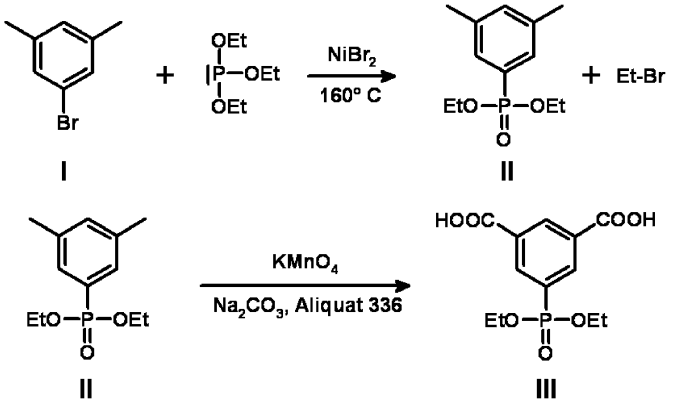

Fig. 1. Synthesis of 5-diethylphosphonoisophthalic acid, $(HOOC)_2C_6H_3$-$PO_3(C_2H_5)_2$ (H_2Et_2L) (III) in two steps starting from 1-bromo-3,5-dimethylbenzene (I).

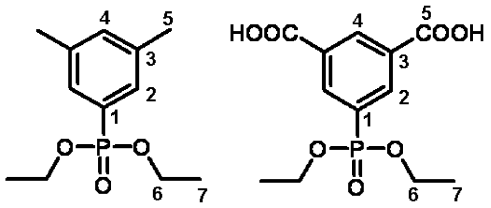

Fig. 2. Labeling scheme of the carbon atoms as used in the NMR section.

viscous liquid was obtained (^{1}H NMR ($CDCl_3$): $\delta = 1.31$ (t, 6H; ^3J (H–H) = 7 Hz, C7H_3), 2.34 (s, 6H; 2× C5H_3), 4.10 (m, 4H, 2× C6H_3), 7.16 (s, 1H, C4-H), 7.41 (d, 2H, 2× C2-H; $^3J_{H-P} = 12.7$ Hz) ppm. ^{13}C NMR ($CDCl_3$): $\delta = 16.3$ (d, C7; $^3J_{C7,P} = 6.5$ Hz), 21.2 (d, C5; $^4J_{C5,P} = 1.3$ Hz), 62.0 (d, C6, $^2J_{C6-P} = 5.4$ Hz), 124.3 (d, C1; $^1J_{C1-P} = 195.4$ Hz), 129.3 (d, C3; $^4J_{C3-P} = 9.8$ Hz), 134.1 (d, C4; $^4J_{C4-P} = 3.3$ Hz) 138.1 (d, C2; $^2J_{C2-P} = 15.8$), 165.6 (d, C5; $^4J_{C5-P} = 2.0$ Hz) ppm. ^{31}P NMR ($CDCl_3$): 20.4 ppm (s)). For labeling of the carbon atoms see Fig. 2.

The oxidation of **II** was performed with $KMnO_4$ according to Ref. [17]. Thus, 2.13 g (8.78 mmol) **II**, 2.51 g (23.7 mmol) Na_2CO_3, 9.30 g (58.83 mmol) $KMnO_4$, and 0.180 ml Aliquat 336 were refluxed for 45 min. The formed MnO_2 was filtered off immediately and washed with hot water. The aqueous phase was cooled in an ice bath and upon acidification with 6 M H_2SO_4, the product crystallizes. The colorless solid was filtered of and washed with cold water (^{1}H NMR (DMSO): $\delta = 1.31$ (t, 6H, ^3J (H–H) = 7 Hz, C7H_3)$_2$), 4.14 (m, 4H, PO(C6H_3), 8.46 (m, 2H, C2-H), 8.70 (m, 1H, C4-H) ppm. ^{13}C NMR (DMSO): $\delta = 16.1$ (d, C7; $^3J_{C7,P} = 5.9$ Hz), 62.2 (d, C6, $^2J_{C6-P} = 5.7$ Hz), 123.0 (d, C1; $^1J_{C1-P} = 188.0$ Hz), 131.9 (d, C2; $^2J_{C2-P} = 14.5$), 133.3 (d, C4; $^4J_{C4-P} = 2.7$ Hz), 135.5 (d, C3; $^4J_{C3-P} = 10.6$ Hz), 165.6 (d, C5; $^4J_{C5-P} = 2.0$ Hz) ppm. ^{31}P NMR (DMSO): 16.4 ppm (s)). For labeling of the carbon atoms see Fig. 2.

2.2. High-throughput experiment, discovery library

The discovery of new compounds in unknown reaction systems is often a time consuming and tedious task. Any time a new ligand is applied in the synthesis of inorganic–organic hybrid compounds the first HT experiment should to be as diverse as possible in order to get an overview on the reaction system and thus, on promising candidates for the synthesis of new crystalline inorganic–organic hybrid compounds. Therefore, H_2Et_2L was reacted with salts of six divalent and trivalent metal cations ($BaCl_2 \cdot 2H_2O$, $CuCl_2 \cdot 2H_2O$, $Co(OAc)_2 \cdot 4H_2O$, $CaCl_2 \cdot 2H_2O$, $AlCl_3 \cdot 6H_2O$, and $SmCl_3 \cdot 6H_2O$) at eight molar ratios M^{n+}:H_2Et_2L:NaOH. The molar ratios of the starting compounds as well as the exact amounts of dosed chemicals is given in the supporting information. The cations were selected based on their difference in ionic charge, ionic radii, and preferred coordination number. The results of the screening of metal salts are shown in

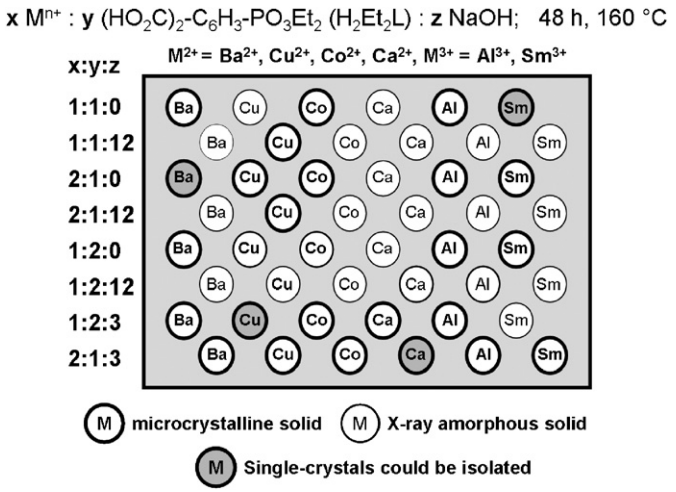

Fig. 3. High-throughput screening in the synthesis of inorganic–organic hybrid compounds: discovery library and the results of the reaction between different metal salts and 5-diethylphophonoisophthalic acid, H_2Et_2L, at eight molar ratios M^{n+}:H_2Et_2L:NaOH = 1:1:0, 1:1:12, 2:1:0, 2:1:12, 1:2:0, 1:2:12, 1:2:3, and 2:1:3, respectively. Bold letters indicate crystalline products; normal letters indicate X-ray amorphous products.

Fig. 3. These results are based on HT powder XRD measurements. From one single HT experiment single-crystals of four new compounds could be isolated and structurally characterized ($[Sm_2(H_2O)_4(H(OOC)_2C_6H_3$-$PO_3)_2]\cdot 2H_2O$ (**1**), $[Cu_3(H_2O)(H(OOC)_2C_6H_3PO_3)_2]\cdot 2H_2O$ (**2**), $Ca_2(H_2O)[H(OOC)_2C_6H_3$-$PO_3H]_2$ (**3**), and $Ba_2(H_2O)_3(OOC)_2C_6H_3$-$PO_3$ (**4**)). So far, only title compounds **1**, **2**, and **3** could be obtained pure phase. In the following, their optimized synthesis procedures are described.

2.3. Synthesis of $[Sm_2(H_2O)_4(H(OOC)_2C_6H_3$-$PO_3)_2]\cdot 2H_2O$ (1)

$[Sm_2(H_2O)_4(H(OOC)_2C_6H_3PO_3)_2]\cdot 2H_2O$ (**1**) was prepared by reacting 3.6 mg (12 μmol) H_2Et_2L, 12 μL (12 μmol) of a 1 M aqueous solution of $SmCl_3\cdot 6H_2O$, 56 μL (143 μmol) of a 2.5 M aqueous solution of KOH, and 181 μL deionized water in a sealed 500 μL Teflon microreactor. The reaction was carried out at 160 °C for 2 days. The resulting light yellow solid was filtered off and washed with deionized water and acetone. X-ray powder diffraction (XRD) experiments confirmed the presence of only one phase, $[Sm_2(H_2O)_4(H(OOC)_2C_6H_3PO_3)_2]\cdot 2H_2O$ (**1**). The corresponding theoretical and experimental powder XRD patterns are given in Fig. S1 in the supporting information. (EDX: Sm:P = 1:1; elemental analysis: found: C, 21.12; H, 2.37. calcd: C, 21.47; H, 2.03).

2.4. Synthesis of $[Cu_3(H_2O)(H(OOC)_2C_6H_3$-$PO_3)_2]\cdot 2H_2O$ (2)

In a reaction of 12 mg (40 μmol) H_2Et_2L with 80 μL 0.5 M aqueous $CuCl_2\cdot 2H_2O$ solution (40 μmol), 80 μL 0.5 M aqueous NaOH solution (40 μmol), and 90 μL H_2O in a Teflon microreactor at 160 °C for 2 days, pure phase solid of $[Cu_3(H_2O)(H(OOC)_2C_6H_3PO_3)_2]\cdot 2H_2O$ (**2**) is obtained. This was confirmed by XRD measurements (Fig. S2). (EDX: Cu:P = 3:2; elemental analysis: found: C, 26.19; H, 1.24. calcd: C, 26.29; H, 1.10).

2.5. Synthesis of $Ca_2(H_2O)[H(OOC)_2C_6H_3$-$PO_3H]_2$ (3)

The reaction of a mixture of 16.8 mg (55.6 μmol) H_2Et_2L, 33 μL (83.5 μmol) 2.5 M NaOH, 37 μL (27.6 μmol) of a 0.75 M aqueous solution of $CaCl_2\cdot 2H_2O$, and 189 μL H_2O at 160 °C for 2 days results in the formation of $Ca_2(H_2O)[H(OOC)_2C_6H_3$-$PO_3H]_2$ (**3**). Powder XRD measurements showed that the product is phase-pure $Ca_2(H_2O)[H(OOC)_2C_6H_3$-$PO_3H]_2$ (**3**) (Fig. S3). (EDX: Ca:P = 1:1; elemental analysis: found: C, 32.15; H, 1.33. calcd: C, 32.77; H, 1.41).

2.6. Physical characterization

XRD patterns were recorded with a STOE STADI P diffractometer using monochromated Cu$K\alpha_1$ radiation. IR spectra were recorded on an ATI Matheson Genesis in the spectral range 4000–400 cm^{-1} using the KBr disk method. Thermogravimetric (TG) analyses were carried out under nitrogen (75 ml min^{-1}, 8 °C min^{-1}) on a Netzsch STA-409CD (**3**) or in air (25 ml min^{-1}, 10 °C min^{-1}) using a NETZSCH STA 449C Analyzer (compounds **1** and **2**). EDX analysis was performed on a Philips ESEM XL 30.

3. Crystallography

The single-crystal structure determination by XRD for compounds **1**, **3**, and **4** was performed on an Enraf Nonius Kappa-CCD diffractometer equipped with a rotating anode (Mo$K\alpha$ radiation, $\lambda = 71.073$ ppm). For data reduction and the absorption correction the program XRED was used [18]. For compound **2**, the data collection was performed on a STOE IPDS diffractometer equipped with a fine-focus sealed-tube X-ray source (Mo$K\alpha$ radiation, $\lambda = 71.073$ ppm). The single-crystal structures of **1**, **2**, and **3** were solved by direct methods; the structure of **4** was solved by the Patterson method. All structures were refined using the program package SHELXTL [19]. All H-atoms bound to carbon atoms were placed onto calculated positions. These H-atoms were refined using a riding model and fixing the temperature factor to be 1.2 times the value of the atom they are bonded to. The crystal data for compounds **1**, **2**, **3** and **4** is listed in Table 1 and selected bond lengths are given in Tables 2–5.

4. Results and discussion

4.1. Crystal structures

4.1.1. Crystal structure of $[Sm_2(H_2O)_4(H(OOC)_2C_6H_3$-$PO_3)_2]\cdot 2H_2O$ (1)

The asymmetric unit of **1** consists of two Sm^{3+} ions, two $[H(OOC)_2C_6H_3$-$PO_3]^{3-}$ anions, four coordinatively bonded

Table 1
Summary of crystal data, intensity measurement, and structure refinement parameters for $[Sm_2(H_2O)_4(H(OOC)_2C_6H_3\text{-}PO_3)_2]\cdot 2H_2O$ (**1**), $[Cu_3(H_2O)(H(OOC)_2C_6H_3\text{-}PO_3)_2]\cdot 2H_2O$ (**2**), $Ca_2(H_2O)[H(OOC)_2C_6H_3\text{-}PO_3H]_2$ (**3**), and $Ba_2(H_2O)_3(OOC)_2C_6H_3\text{-}PO_3$ (**4**)

Compound	**1**	**2**	**3**	**4**
Crystal system	Triclinic	Monoclinic	Monoclinic	Triclinic
Space group	$P-1$	I2/a	$P2_1$	$P-1$
a (pm)	706.51(3)	964.6(1)	897.71(2)	690.87(1)
b (pm)	1097.85(6)	1727.4(1)	1237.17(3)	880.18(2)
c (pm)	1611.71(6)	1303.4(1)	907.97(2)	1112.62(2)
α (°)	109.700(3)			92.031(1)
β (°)	91.681(3)	110.81(1)	104.088(1)	102.5740(1)
γ (°)	93.868(2)			95.074(2)
Volume (10^6 pm^3)	1172.45(9)	2030.2(3)	978.08(4)	656.72(2)
Z	2	4	2	2
Formula mass (g/mol)	894.96	730.83	586.36	570.80
ρ (g/cm^3)	2.535	2.391	1.991	2.887
$F(000)$	860	1452	596	528
Crystal size (mm^3)	$0.16\times0.05\times0.04$	$0.34\times0.15\times0.09$	$0.24\times0.15\times0.09$	$0.2\times0.15\times0.09$
μ (mm^{-1})	5.197	3.370	0.834	6.131
Abs. correction	Numerical	Numerical	Numerical	Numerical
$T_{min.}/T_{max.}$	0.7449/0.9155	0.8578/0.9524	0.9370/0.9725	0.6467/0.4665
θ Range (°)	3.26–27.46	2.36–27.93	3.29–27.48	3.20–27.55
Range in $h\,k\,l$	$-9\leqslant h\leqslant 9$, $-14\leqslant k\leqslant 14$, $-20\leqslant l\leqslant 20$	$-12\leqslant h\leqslant 12$, $-22\leqslant k\leqslant 22$, $-17\leqslant l\leqslant 17$	$-11\leqslant h\leqslant 11$, $-16\leqslant k\leqslant 15$, $-11\leqslant l\leqslant 11$	$-8\leqslant h\leqslant 8$, $-11\leqslant k\leqslant 11$, $-14\leqslant l\leqslant 14$
Total data collect.	16010	8700	15744	9273
Unique/obs. data ($I > 2\sigma(I)$)	5209/3833	2315/2039	4455/4006	2975/2757
Extinction coeff.	–	0.0023(3)	–	0.0122(8)
Flack parameter	–	–	−0.02(3)	–
R(int)	0.0672	0.0315	0.0392	0.0312
$R1$, $wR2$ ($I > 2\sigma(I)$)	0.0558, 0.1173	0.0258, 0.0687	0.0340, 0.0741	0.0212, 0.0618
$R1$, $wR2$ (all data)	0.0881, 0.1308	0.0304, 0.0699	0.0430, 0.0788	0.0258, 0.0804
Goodness of fit	1.041	1.061	1.086	1.263
No. of variables	364	196	360	191
Δe min/max (eÅ^{-3})	−2.606/2.066	−0.901/1.508	−0.428/0.350	−1.279/1.092

Table 2
Selected bond lengths (Å) for $[Sm_2(H_2O)_4(H(OOC)_2C_6H_3\text{-}PO_3)_2]\cdot 2H_2O$ (**1**)

Sm–O	2.316(7)–2.632(7)	P–O	1.501(7)–1.553(7)
P–C	1.807(11), 1.803(10)	C–C_{phenyl}	1.376(14)–1.405(14)
C–C	1.488(14)–1.506(14)	C–O	1.219(13)–1.326(12)

Table 3
Selected bond lengths (Å) for $[Cu_3(H_2O)(H(OOC)_2C_6H_3\text{-}PO_3)_2]\cdot 2H_2O$ (**2**)

Cu–O	1.885(2)–2.156(2)	P–O	1.520(2)–1.553(2)
P1–C1	1.805(2)	C–C_{phenyl}	1.390(3)–1.397(3)
C–C	1.492(3), 1.493(3)	C–O	1.206(3)–1.327(3)

Table 4
Selected bond lengths (Å) for $Ca_2(H_2O)[H(OOC)_2C_6H_3\text{-}PO_3H]_2$ (**3**)

Ca–O	2.299(2)–2.631(2)	P–O	1.501(2)–1.589(2)
P–C	1.801(3), 1.806(3)	C–C_{phenyl}	1.384(4)–1.406(4)
C–C	1.477(4)–1.510(3)	C–O	1.218(3)–1.325(3)

Table 5
Selected bond lengths (Å) for $Ba_2(H_2O)_3(OOC)_2C_6H_3\text{-}PO_3$ (**4**)

Ba–O	2.685(3)–3.4062(10)	P–O	1.519(3)–1.542(3)
P–C	1.811(4)	C–C_{phenyl}	1.272(5)–1.401(5)
C–C	1.504(5), 1.505(5)	C–O	1.254(5)–1.262(5)

water molecules, and two lattice water molecules (Fig. S4). The protons of both carboxylic acid groups have been located unequivocally from the difference Fourier map and were refined using a riding model and fixing the temperature factor to be 1.2 times the value of the atom they are bonded to. Both Sm^{3+} ions are coordinated by nine oxygen atoms. The coordination behavior of the organic molecules is shown in Fig. 4. In each molecule, the phosphonic acid is fully deprotonated, one carboxylic acid group, and one carboxylate group is present. The C7- and C15-carboxylic acid groups form hydrogen bonded dimmers with oxygen atoms O4 and O11 as H-donors and oxygen atoms O5 and O12 as H-acceptors which act additionally as H-acceptors in hydrogen bonding with water molecules O15 and O16. The C8 and C16-carboxylate groups act as chelating ligands with Sm1 and Sm2, respectively. The P1- and P2-phosphonate groups coordinate to both Sm1 and Sm2. Whereas three water molecules (O15, O17, and O18) are coordinating to Sm1, Sm2 is

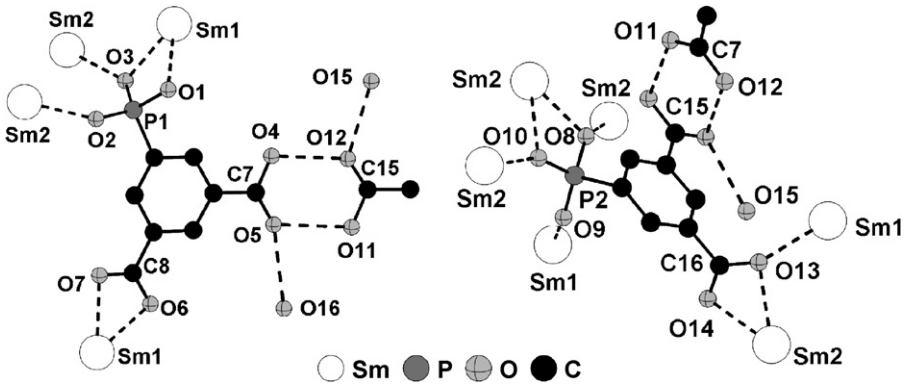

Fig. 4. Coordination behavior of the HL^{3-} ions in $[Sm_2(H_2O)_4(H(OOC)_2C_6H_3\text{-}PO_3)_2]\cdot 2H_2O$ (**1**). H-atoms are omitted for clarity.

coordinated by only one water molecule (O19) (Fig. S5). The structure of **1** can be described as follows: edge-sharing $Sm2O_9$ polyhedra form chains along the *a*-axis with sidearms of edge-sharing $Sm1O_9$ polyhedra (Fig. 5). The organic molecules are oriented perpendicular to these chains (Fig. S6). Thus, the chains are interconnected along the *b*-axis by phosphonate and carboxylate groups coordinating to Sm^{3+} ions. In contrast, along the *c*-axis these chains are interconnected by hydrogen bonding between two carboxylic acid groups. Thus, one-dimensional channels along the *a*-axis are formed which contain hydrogen bonded water molecules (Fig. 6).

4.1.2. Crystal structure of $[Cu_3(H_2O)(H(OOC)_2C_6H_3\text{-}PO_3)_2]\cdot 2H_2O$ (2)

The asymmetric unit of $[Cu_3(H_2O)(H(OOC)_2C_6H_3\text{-}PO_3)_2]\cdot 2H_2O$ (**2**) is given in Fig. S7. It is comprised of one Cu^{2+} ion on a special position (Cu1) and one on a general position (Cu2), one $[H(OOC)_2C_6H_3\text{-}PO_3]^{3-}$ ion and two water molecules O7 (general position) and O8 (special position). All protons bound to oxygen atoms could be located unequivocally from the Fourier difference map and were refined freely. The phosphonic acid group is fully deprotonated and whereas oxygen atom O2 acts as μ_2-ligand bridging the Cu1 and Cu2 ions, the oxygen atoms O1 and O3 coordinate only to one Cu2 ion each (Fig. 7). The C7-carboxylic acid group acts as a H-donor with the phosphonate oxygen atom O3 and as a H-acceptor in a hydrogen bond with the water molecule O9. The C8-carboxylate group is involved in the coordination of two different Cu^{2+} ions (Fig. 7). Cu1 is coordinated by five oxygen atoms and Cu2 by four oxygen atoms. Cu_3O_{11} trimers are formed by one CuO_5- and two CuO_4 corner-sharing polyhedra (Fig. S8), which are connected by phosphonate groups to form chains along the *a*-axis (Fig. 8). Around these chains the organic molecules are arranged (Fig. S9), which further connect the chains in the *b*- and *c*-direction (Fig. 9).

4.1.3. Crystal structure of $Ca_2(H_2O)[H(OOC)_2C_6H_3\text{-}PO_3H]_2$ (3)

The asymmetric unit of $Ca_2(H_2O)[H(OOC)_2C_6H_3\text{-}PO_3H]_2$ (**3**) consists of two Ca^{2+} ions, two

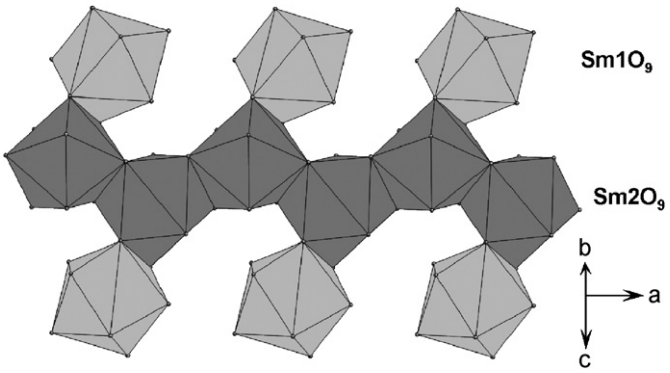

Fig. 5. Edge-sharing $Sm2O_9$ polyhedra form chains along the *a*-axis with edge-sharing $Sm1O_9$ polyhedra as sidearms as observed in $[Sm_2(H_2O)_4(H(OOC)_2C_6H_3\text{-}PO_3)_2]\cdot 2H_2O$ (**1**).

$[H(OOC)_2C_6H_3\text{-}PO_3H]^{2-}$ ions and one water molecule (Fig. S10). The protons belonging to carboxylic- and hydrogenphoshonic acid groups (O4, O11, O3, and O9) could be located unambiguously from the Fourier difference map and were refined freely. The coordination behavior of the H_2L^{2-} ions is shown in Fig. 10. Each organic molecule is twofold deprotonated leading to the presence of one carboxylate, one carboxylic-, and one mono-hydrogenphosphononic acid group. The carboxylate groups act as chelating ligands, and at the same time one oxygen is bridging two Ca^{2+} ions (μ_2-oxygen atoms O6 and O13). Both carboxylic acid groups are pseudo bridging. Thus, the carbonyl oxygen atom coordinates to a Ca^{2+} ion and at the same time, the OH-group acts as H-donor in a hydrogen bond with an oxygen atom coordinating to the respective Ca^{2+} ion. Whereas the P1-hydrogenphosphonic acid group is coordinating to two Ca^{2+} ions, the P2-hydrogenphosphonic acid group is coordinating to three Ca^{2+} ions. Both hydrogenphosphonic acid groups are involved in hydrogen bonding. Both Ca^{2+} ions are coordinated by seven oxygen atoms and form Ca_2O_{12}-dimers by sharing edges (Fig. S11). These dimers are connected by both P1- and P2-hydrogenphosphonate groups to form layers in the *b*, *c*-plane (Fig. 11) that are further connected along the *a*-axis by the organic units (Fig. 12).

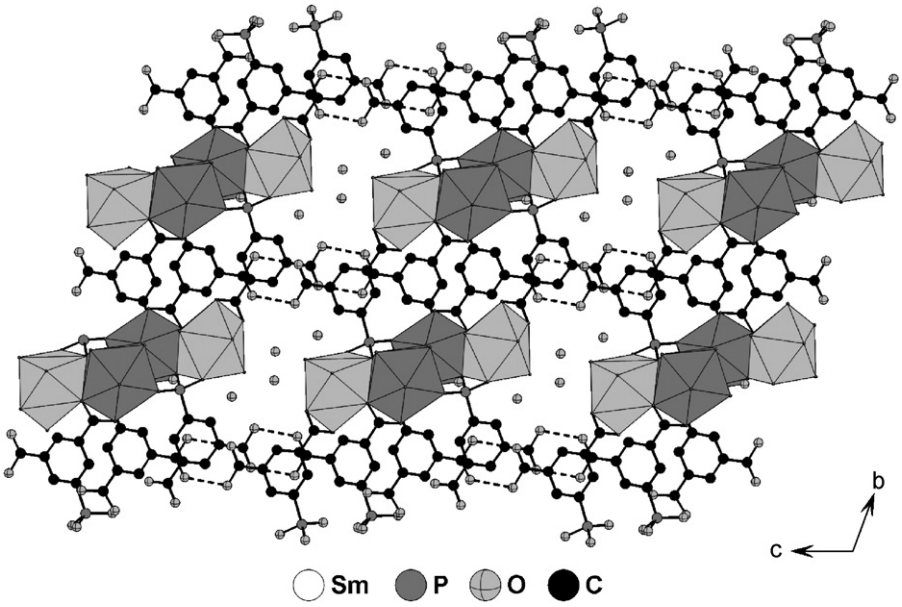

Fig. 6. In $[Sm_2(H_2O)_4(H(OOC)_2C_6H_3\text{-}PO_3)_2]\cdot 2H_2O$ (**1**) chains of edge-sharing SmO9 polyhedra are connected by coordinative (along the *b*-axis) as well as hydrogen bonds (dashed lines, along the *c*-axis). Thus, one-dimensional channels along the *a*-axis with hydrogen bound water molecules are formed. ($Sm1O_9$ polyhedra are presented in light gray and $Sm2O_9$ polyhedra in dark gray).

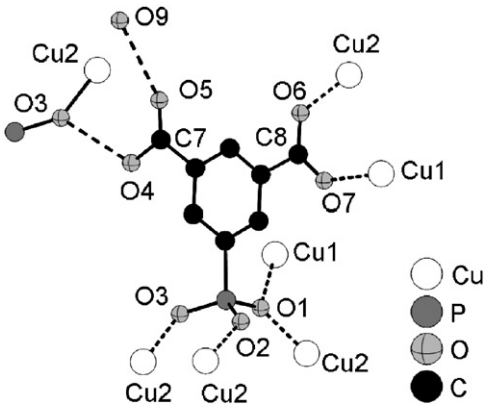

Fig. 7. Coordination behavior of the HL^{3-} ions in $[Cu_3(H_2O)(H(OOC)_2C_6H_3\text{-}PO_3)_2]\cdot 2H_2O$ (**2**). H-atoms are omitted for clarity.

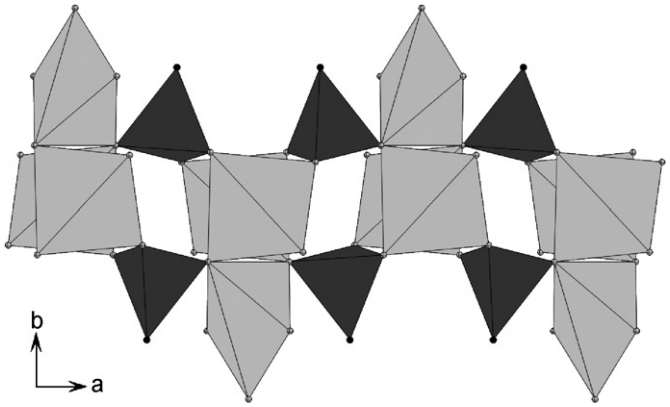

Fig. 8. In $[Cu_3(H_2O)(H(OOC)_2C_6H_3\text{-}PO_3)_2]\cdot 2H_2O$ (**2**), trimers of Cu_3O_{11} (light gray polyhedra) are connected by phosphonate groups (dark gray polyhedra) to form chains along the *a*-axis.

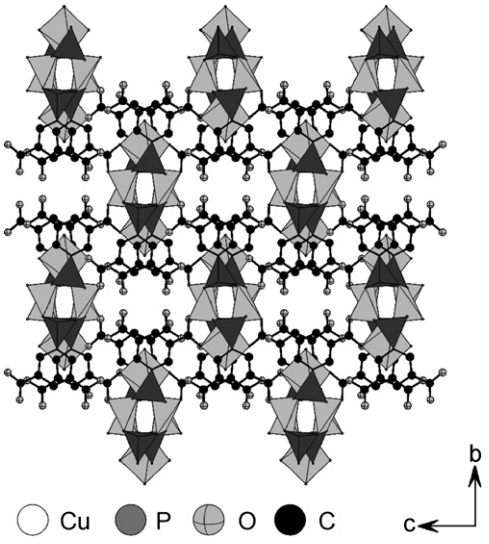

Fig. 9. In $[Cu_3(H_2O)(H(OOC)_2C_6H_3\text{-}PO_3)_2]\cdot 2H_2O$ (**2**), the copper phosphonate chains along the *a*-axis are connected by HL^{3-} ions in the *b*- and *c*-direction.

*4.1.4. Crystal structure of $Ba_2(H_2O)_3(OOC)_2C_6H_3\text{-}PO_3$ (**4**)*

The asymmetric unit of $Ba_2(H_2O)_3(OOC)_2C_6H_3\text{-}PO_3$ (**4**) is shown in Fig. S12. It consists of two Ba^{2+} ions, one $[(OOC)_2C_6H_3\text{-}PO_3]^{4-}$ anion and three water molecules. All oxygen atoms are involved in the coordination of the Ba^{2+} ions. The coordination behavior of the organic molecule is given in Fig. 13. The C7-carboxylate group is coordinating to three Ba^{2+} ions. Whereas oxygen atom O5 coordinates to one Ba^{2+} ion, oxygen atom O4 acts as a μ_2-bridging ligand. The C8-carboxylate group coordinates in a bridging

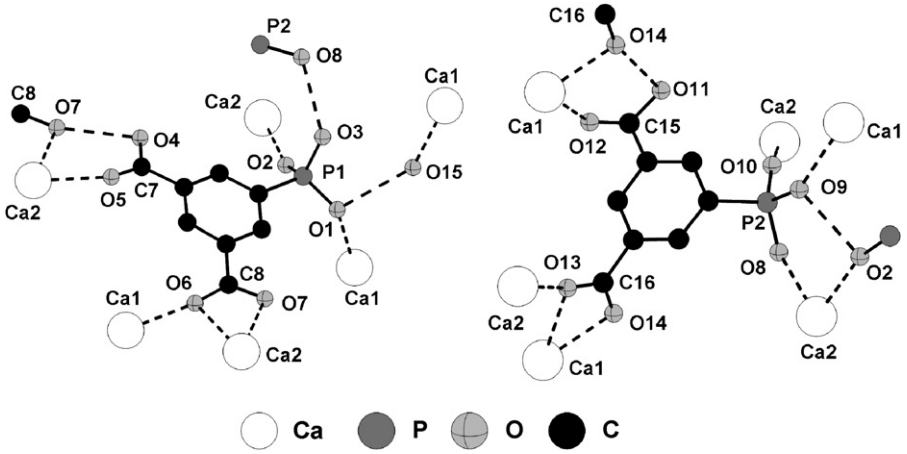

Fig. 10. Coordination behavior of the H_2L^{2-} ions in $Ca_2(H_2O)[H(OOC)_2C_6H_3\text{-}PO_3H]_2$ (**3**). H-atoms are omitted for clarity.

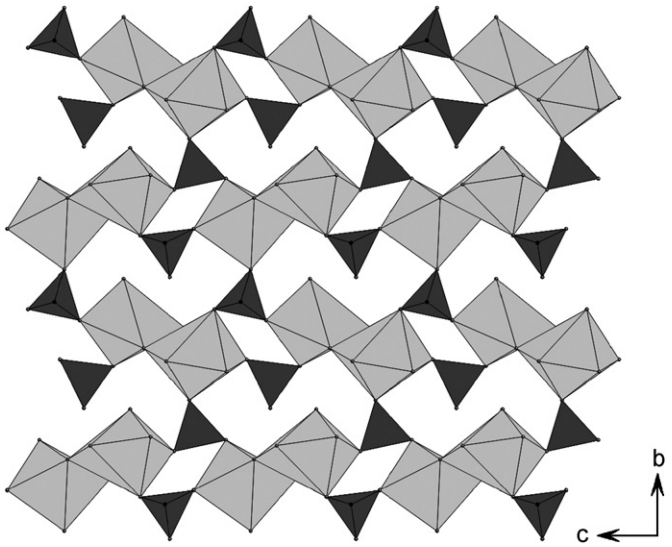

Fig. 11. In $Ca_2(H_2O)[H(OOC)_2C_6H_3\text{-}PO_3H]_2$ (**3**), Ca_2O_{12} dimers (light gray) are connected by hydrogenphosphonate groups (dark gray) to form layers in the *b*, *c*-plane.

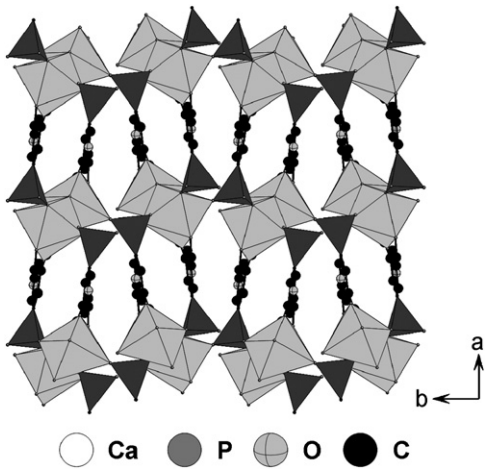

Fig. 12. Calcium-hydrogenphosphonate layers are connected by H_2L^{3-} ions along the *a*-axis, as observed in $Ca_2(H_2O)[H(OOC)_2C_6H_3\text{-}PO_3H]_2$ (**3**). (Ca_2O_{12} dimers are presented inlight gray and hydrogenphosphonate groups in dark gray).

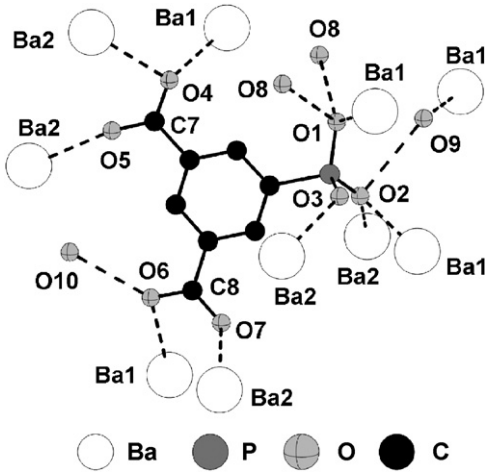

Fig. 13. Coordination behavior of the L^{4-} ions in $Ba_2(H_2O)_3(OOC)_2C_6H_3\text{-}PO_3$ (**4**). H-atoms are omitted for clarity.

mode two Ba^{2+} ions, and additionally acts as H-acceptor in a hydrogen bond with the water molecule O10. The phosphonate group is involved in the coordination of four Ba^{2+} ions and in hydrogen bonding with three water molecules. $Ba1O_9$- and $Ba2O_8$ polyhedra form face-sharing Ba_2O_{14} dimers (Fig. S13) which are further connected to each other by sharing edges to form inorganic Ba–O-layers in the *a*, *c*-plane (Fig. 14). These layers are connected along the *b*-axis via the organic molecules (Fig. 15).

4.2. IR spectroscopy

The title compounds **1**, **2** and **3** were characterized using IR-spectroscopy (Fig. 16). They all exhibit very similar vibration bands, which are hard to assign in detail. Nevertheless, important information can be deduced. Thus, in the following, only bands related to the presence of water molecules, and carboxylic acid or carboxylate groups are discussed in detail. The IR-spectra of all compounds exhibit typical bands in the region between 1250 and 980 cm^{-1} that are due to the P–C and P–O stretching vibrations of the tetrahedral CPO_3-group. The

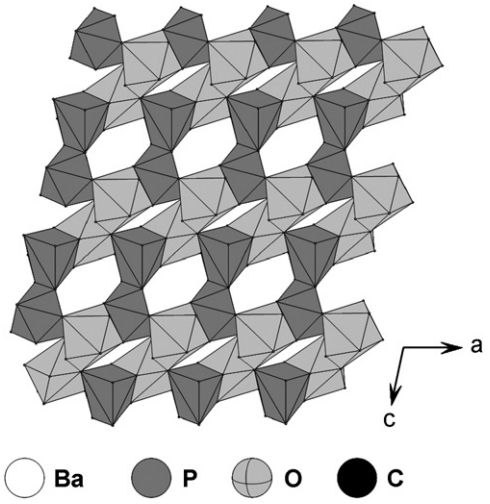

Fig. 14. In $Ba_2(H_2O)_3(OOC)_2C_6H_3\text{-}PO_3$ (**4**), face-sharing Ba_2O_{14} dimers are connected by sharing edges. Thus, inorganic Ba–O-layers in the *a*, *c*-plane are formed. ($Ba1O_9$ polyhedra are presented in light gray and $Ba2O_8$ polyhedra are presented in dark gray).

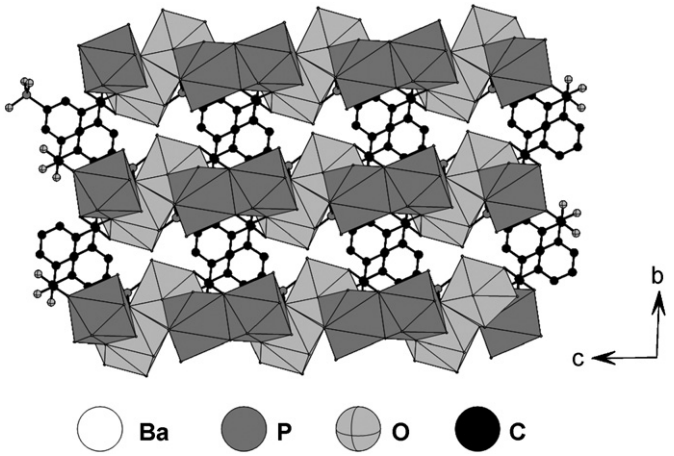

Fig. 15. The Ba–O-layers are connected along the *b*-axis via L^{4-} ions, as observed in $Ba_2(H_2O)_3(OOC)_2C_6H_3\text{-}PO_3$ (**4**). ($Ba1O_9$ polyhedra are presented in light gray and $Ba2O_8$ polyhedra are presented in dark gray).

symmetric and antisymmetric C–H stretching vibrations of the aromatic ring result in two bands of low intensity in the region between 3100 and 3000 cm^{-1}. Schemes of typical coordination modes observed for carboxylic acids are given in Fig. 17.

Bands above 3100 cm^{-1} in the IR-spectrum of $[Sm_2(H_2O)_4(H(OOC)_2C_6H_3\text{-}PO_3)_2]\cdot 2H_2O$ (**1**) show the presence of water molecules in the structure. Whereas the broad band with a maximum 3370 cm^{-1} is due the O–H stretching vibration of water molecules involved in H–bonds, the sharp band at 3610 cm^{-1} can be assigned to the O–H stretching vibration of water molecules coordinated to Sm^{3+} ions. A broad band at 1697 cm^{-1} is due to the overlap the C=O stretching vibrations of the two crystallographically independent carboxylic acid groups. The two different coordination modes of the

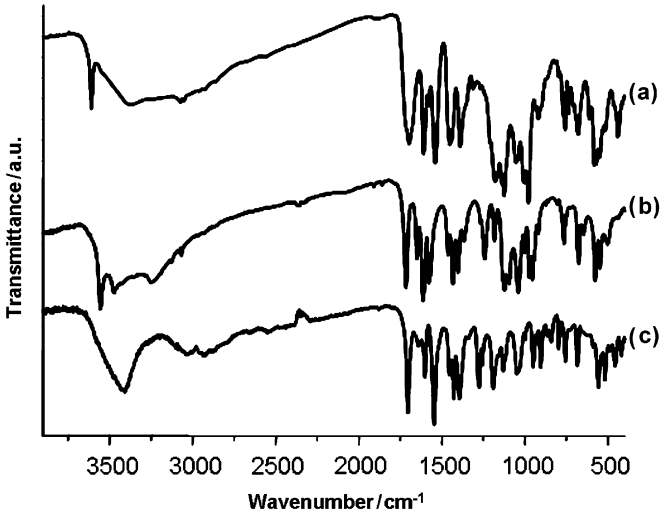

Fig. 16. IR-spectra for (a) $[Sm_2(H_2O)_4(H(OOC)_2C_6H_3\text{-}PO_3)_2]\cdot 2H_2O$ (1), (b) $[Cu_3(H_2O)(H(OOC)_2C_6H_3\text{-}PO_3)_2]\cdot 2H_2O$ (2), and (c) $Ca_2(H_2O)[H(OOC)_2C_6H_3\text{-}PO_3H]_2$ (3).

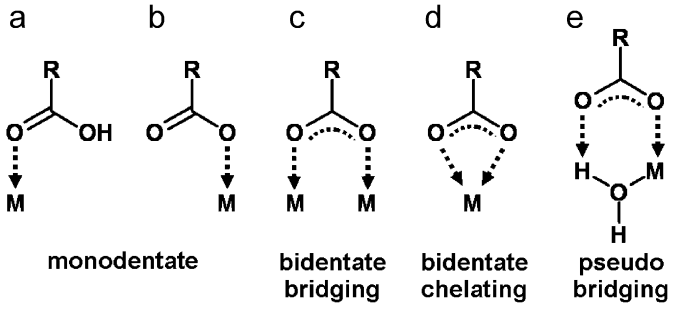

Fig. 17. Typical coordination modes of carboxylic acids [20,21].

carboxylate groups result in two additional sets of bands at 1609/1452 cm^{-1} and 1539/1389 cm^{-1}. They are due to a bidentate bridging (Fig. 17c) and a bidentate chelating (Fig. 17d) interaction between the carboxylate groups and the Sm^{3+} ions [20,21].

According to crystallographic results, several bands above 3100 cm^{-1} due O–H stretching vibrations in the IR-spectrum of $[Cu_3(H_2O)(H(OOC)_2C_6H_3\text{-}PO_3)_2]\cdot 2H_2O$ (**2**) show the presence of water molecules coordinated to Cu^{2+} ions (a sharp band at 3556 cm^{-1}) as well as hydrogen bonded water molecules. The C=O stretching vibration of the carboxylic acid group results in a band at 1715 cm^{-1}. The bands due the bidentate bridging interaction (Fig. 17c) of the carboxylate group with the Cu^{2+} ions can be assigned to the bands located at 1578 and 1402 cm^{-1} [20,21].

A broad band due to the O–H stretching vibration in the IR-spectrum of $Ca_2(H_2O)[H(OOC)_2C_6H_3\text{-}PO_3H]_2$ (**3**) indicates the presence of water molecules in the structure. The C=O stretching vibration of the carboxylic acid group results in a sharp band of high intensity at 1704 cm^{-1}. Bands at 1557 and 1394 might be due to the bidentate

bridging interaction (Fig. 17c) of the carboxylate groups with the Ca^{2+} ions [20,21].

4.3. Thermal properties

The thermal properties of the title compounds **1**, **2** and **3** were studied using TG analysis (see supporting information).

According to TG measurements, the water molecules in $[Sm_2(H_2O)_4(H(OOC)_2C_6H_3\text{-}PO_3)_2]\cdot 2H_2O$ (**1**) are released in two steps (Fig. S14). Thus, up to 180 °C a weight loss of 8.0% is observed which corresponds to the release of four water molecules per formula unit (calcd. 8.1%). In a second step, up to 370 °C a total weight loss of 13.5% occurs. The calculated value for the release of all six water molecules per formula unit is only 12.1%. The higher weight loss can be explained by a starting condensation of the carboxylic acid groups accompanied by the release of additional water molecules. A steep weight loss starting from 430 °C indicates the collapse of the structure.

In the TG diagram of $[Cu_3(H_2O)(H(OOC)_2C_6H_3\text{-}PO_3)_2]\cdot 2H_2O$ (**2**) up to 240 °C no weight loss is observed (Fig. S15). The three water molecules per formula unit are released in a single step from 240 to 320 °C (weight loss of 7.7%; calcd.: 7.3%). A steep weight loss starting from 350 °C indicates the collapse of the structure. Upon further heating several steps of weight loss occur due to the degradation of the compound.

The TG diagram of $Ca_2(H_2O)[H(OOC)_2C_6H_3\text{-}PO_3H]_2$ (**3**) shows in the first step a weight loss starting from 230 to 430 °C (Fig. S16). The value of 6.1% (calcd. 6.1%) corresponds to the departure of two water molecules per formula unit. Thus, not only the lattice water molecules are released but also water from the condensation of hydrogenphosphonate and carboxylic acid groups. Upon further heating above 430 °C, a continuous weight loss with two steps due to further condensation and pyrolysis of the organic part is observed.

5. Conclusion

We have synthesized a new ligand, 5-diethylphosphonoisophthalic acid ($(HOOC)_2C_6H_3\text{-}PO_3(C_2H_5)_2$, H_2Et_2L) and used in the synthesis of new metal phosphonates. Using HT methods, we have successfully screened several metal salts for the synthesis of new crystalline metal phosphonates. Thus, from a discovery library single crystals of four new compounds, $[Sm_2(H_2O)_4(H(OOC)_2C_6H_3\text{-}PO_3)_2]\cdot 2H_2O$ (**1**), $[Cu_3(H_2O)(H(OOC)_2C_6H_3\text{-}PO_3)_2]\cdot 2H_2O$ (**2**), $Ca_2(H_2O)[H(OOC)_2C_6H_3\text{-}PO_3H]_2$ (**3**), and $Ba_2(H_2O)_3(OOC)_2C_6H_3\text{-}PO_3$ (**4**), could be isolated and their crystal structures have been elucidated. The new ligand containing two carboxylic acid groups and one phosphonate group, has shown to be very versatile in its coordination behavior (Fig. 18). In the title compounds carboxylic acid-, carboxylate-, hydrogenphosphonate-, as well as phosphonate groups with different types of interaction with metal ions are observed (bidentate bridging, bidentate chelating, μ_2-oxygen bridging, as well as monodentate-coordinating). Looking at the structures of the title compounds, one finds different metal–oxygen–metal (M–O–M) connectivities. Thus, in $Ca_2(H_2O)[H(OOC)_2C_6H_3\text{-}PO_3H]_2$ (**3**), Ca_2O_{12}-dimers are present which are connected by hydrogenphosphonate groups to form layers. In $[Cu_3(H_2O)(H(OOC)_2C_6H_3\text{-}PO_3)_2]\cdot 2H_2O$ (**2**), Cu_3O_{11} trimers are observed which are further connected into chains by phosphonate groups. In $[Sm_2(H_2O)_4(H(OOC)_2C_6H_3\text{-}PO_3)_2]\cdot 2H_2O$ (**1**), infinite Sm–O–Sm chains are connected by the linker molecules. Thus, one-dimensional channels are formed which are occupied by water molecules. Finally, in $Ba_2(H_2O)_3(OOC)_2C_6H_3\text{-}PO_3$ (**4**) infinite Ba–O–Ba-layers are observed. Thus,

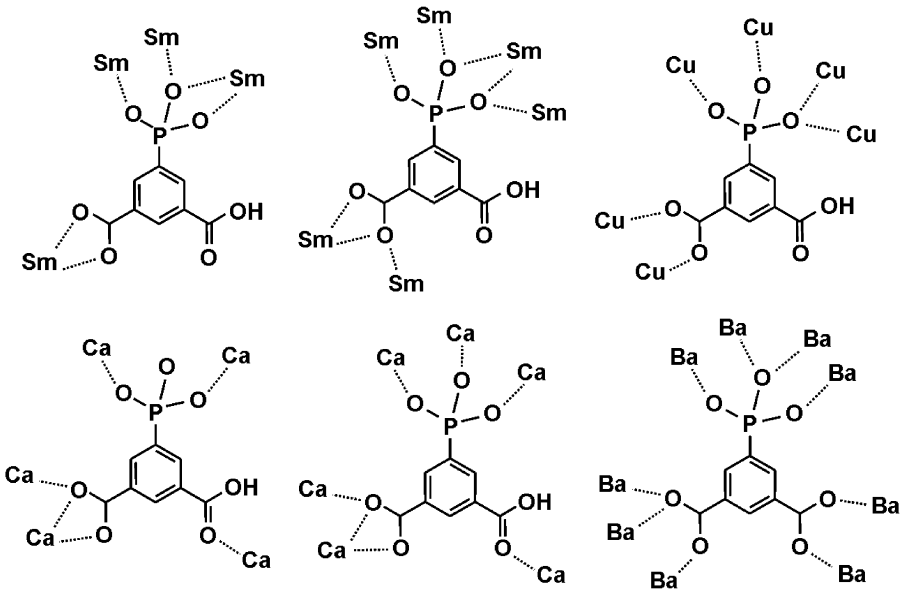

Fig. 18. Schematic presentation of the coordination modes of the organic molecules as observed in the title compounds.

the last two structures belong to the family of hybrid metal oxides with infinite M–O–M arrays, while the first two compounds can be assigned to the family of coordination polymers according to the nomenclature proposed by Cheetham et al. [2]. The ability to form such extended solids in combination with H_4L is probably due to the higher preferred coordination number of the Sm^{3+} and Ba^{2+} ions. Furthermore, the high coordination flexibility of the phosphonic acid group might prevent the formation of secondary building units as observed in carboxylate chemistry that could lead to tailored synthesis of phosphonate based metal-organic framework structures. Future work will address the systematic investigation of the individual systems M^{n+}/H_2Et_2L/Base in order to extract reaction as well as structural trends.

Supplementary material

Molar ratios and dispensed amounts for the HT metal screening, additional figures for the structure description, as well as experimental and theoretical XRD patterns for the title compounds **1**, **2**, and **3**. Crystallographic data for the structures (CCDC 649041 (**1**), CCDC 649042 (**2**), CCDC 649043 (**3**), and CCDC 649044 (**4**)) have been deposited with the Cambridge Crystallographic Data Centre. Copies of the data can be obtained free of charge on application to The Director, CCDC, 12 Union Road, Cambridge CB2 1EZ, UK (Fax: int.code_(1223)336-033; e-mail for inquiry: fileserv@ccdc.cam.ac.uk.

Acknowledgments

The authors thank Dr. P. Mayer, University of Munich, for the acquisition of the single-crystal data. Financial support by the Deutsche Forschungsgemeinschaft through the Project STO 643/2 is gratefully acknowledged.

Appendix A. Supplementary material

Supplementary data associated with this article can be found in the online version at doi:10.1016/j.jssc.2007.08.026.

References

[1] S. Kitagawa, R. Kitaura, S.-I. Noro, Angew. Chem. Int. Ed. 43 (2004) 2338.
[2] A.K. Cheetham, C.N.R. Rao, R.K. Feller, Chem. Commun. (2006) 4780.
[3] U. Mueller, M. Schubert, F. Teich, H. Puetter, K. Schierle-Arndt, J. Pastre, J. Mater. Chem. 16 (2006) 626.
[4] K. Maeda, Microporous Mesoporous Mater 73 (2004) 47.
[5] M. Eddaoudi, D.B. Moler, H. Li, B. Chen, T.M. Reineke, M. O'Keeffe, O.M. Yaghi, Acc. Chem. Res. 34 (2001) 319.
[6] G. Ferey, J. Solid State Chem. 152 (2000) 37.
[7] S.S.Y. Chui, S.M.F. Lo, J.P.H. Charmant, A.G. Orpen, I.D. Williams, Science (Washington, DC) 283 (1999) 1148.
[8] G. Ferey, C. Serre, C. Mellot-Draznieks, F. Millange, S. Surble, J. Dutour, I. Margiolaki, Angew. Chem. Int. Ed. 43 (2004) 6296.
[9] N. Stock, T. Bein, J. Mater. Chem. 15 (2005) 1384.
[10] N. Stock, N. Guillou, T. Bein, G. Ferey, Solid State Sci. 5 (2003) 629.
[11] N. Stock, M. Rauscher, T. Bein, J. Solid State Chem. 177 (2004) 642.
[12] S. Bauer, N. Stock, Angew. Chem. Int. Ed. Angew. Chem. Int. Ed. 46 (2007) 6857.
[13] S. Bauer, C. Serre, T. Devic, P. Horcajada, J. Marrot, G. Férey, N. Stock, submitted for publication.
[14] S. Bauer, T. Bein, N. Stock, Inorg. Chem. 44 (2005) 5882.
[15] N. Stock, T. Bein, Angew. Chem. Int. Ed. 43 (2004) 749.
[16] P. Travs, Chem. Ber. 103 (1970) 2428.
[17] H.G. Becker, W. Berger, G. Domaschke, Organikum, 20 ed., Wiley-VCH Verlag GmbH & Co., KGaA, Weinheim, 1999.
[18] XRED, Data Reduction and Absorption Correction Program Version 1.09 for Windows, Stoe and Cie GmbH, Darmstadt, 1997.
[19] G.M. Sheldrick, in SHELXTl-PLUS Crystallographic System, Siemens Analytical X-ray Instruments Inc., Madison, WI, 1992.
[20] L.J. Bellamy, Infrared Spectra of Complex Molecules, Wiley, New York, 1958.
[21] A.S. Milev, G.S.K. Kannangara, M.A. Wilson, Langmuir 20 (2004) 1888.